Journal of Saudi Chemical Society (2016) **xxx**, xxx–xxx

King Saud University

Journal of Saudi Chemical Society

www.ksu.edu.sa
www.sciencedirect.com

ORIGINAL ARTICLE

A comparative study of key properties of glycine glycinium picrate (GGP) and glycinium picrate (GP): A combined experimental and quantum chemical approach

Mohd. Shkir [a,b,*], Shabbir Muhammad [a,b,*], S. AlFaify [a,b], Ahmad Irfan [b,c], M. Ajmal Khan [a], Abdullah G. Al-Sehemi [b,c], I.S. Yahia [a], Budhendra Singh [e], Igor Bdikin [d,e]

[a] *Department of Physics, College of Science, King Khalid University, Abha 61413, P.O. Box 9004, Saudi Arabia*
[b] *Research Center for Advanced Materials Science (RCAMS), King Khalid University, Abha 61413, P.O. Box 9004, Saudi Arabia*
[c] *Department of Chemistry, Faculty of Science, King Khalid University, Abha 61413, P.O. Box 9004, Saudi Arabia*
[d] *National Research University of Electronic Technology, "MIET" Bld. 1, Shokin Square, 124498, Moscow, Russia*
[e] *TEMA-NRD, Mechanical Engineering Department and Aveiro Institute of Nanotechnology (AIN), University of Aveiro, 3810-193 Aveiro, Portugal*

Received 21 September 2015; revised 20 April 2016; accepted 3 May 2016

KEYWORDS

Crystal growth;
Nanoindentation;
Hardness measurement;
Photophysical properties;
Density functional theory

Abstract Using experimental and computational techniques, a comparative study of electro-optical properties for glycine glycinium picrate (GGP) and glycinium picrate (GP) compounds has been performed. The single crystal of GGP has been grown using slow evaporation technique that was further subjected to experimental characterization of its electro-optical properties. The good optical transparency and mechanical strength at micro level was confirmed from optical and nanoindentation measurements using the Oliver–Pharr method of the grown single crystals. Differential scanning calorimetric (DSC) analysis was done to probe the thermal stability of the grown single crystals. Using the density functional theory (DFT) methods, we have not only investigated the GGP but also proposed GP molecule. Additionally, we have shed light on the molecular geometries, infrared and Raman spectra, linear and nonlinear optical properties of both GGP and GP at molecular level. The time dependent DFT (TD-DFT) approach was adopted to calculate the excitation energies of the molecules in different phases including gas, water, acetone, cyclohexane

* Corresponding authors at: Department of Physics, College of Science, King Khalid University, Abha, Saudi Arabia.
E-mail addresses: shkirphysics@gmail.com, shkirphysics@kku.edu.sa (Mohd. Shkir), shabbir193rb@gmail.com (S. Muhammad).
Peer review under responsibility of King Saud University.

ELSEVIER Production and hosting by Elsevier

http://dx.doi.org/10.1016/j.jscs.2016.05.003

Please cite this article in press as: M. Shkir et al., A comparative study of key properties of glycine glycinium picrate (GGP) and glycinium picrate (GP): A combined experimental and quantum chemical approach, Journal of Saudi Chemical Society (2016), http://dx.doi.org/10.1016/j.jscs.2016.05.003

and chloroform as well. For GGP, its wavelength of maximum absorption is calculated to be ~390 nm at B3LYP/6-31G* level of theory. The calculated amplitudes of first hyperpolarizability (β_{tot}) for GGP and GP are found to be 712 and 970 a. u., respectively, which are about 16 and 23 times larger than that of the urea molecule (a prototype NLO molecule). Thus the present study not only brings to limelight the optical and nonlinear optical properties of GGP but also sheds light on the possible potential of GP as new NLO molecule.

1. Introduction

As per the current demand of modern technology the organic optical materials are very important for various device applications like semiconductors, e.g., optoelectronics, photonics, and superconductors etc. [1–6]. Optical materials gain attention in recent years with respect to their future potential applications in the field of optoelectronic such as optical communication, optical computing, optical switching, and dynamic image processing [5,7–10]. Due to π-conjugation the organic materials display a number of significant optical properties [11–13]. Organic materials have been of particular interest because the nonlinear optical response in this broad class of materials is microscopic in origin, offering an opportunity to use theoretical modeling coupled with synthetic flexibility to design and produce novel materials [14–16]. Also, organic nonlinear optical materials are attracting a great deal of attention, as they have large optical susceptibilities, inherent ultrafast response times, and high optical thresholds for laser power as compared with inorganic materials [17]. Glycine glycinium picrate is a well known material and many reports are available in the literature with different other names like GP and GGP/DGP [18–23]. Recently, glycinium picrate (GP) was reported with very few properties as a new compound and found noticeable second harmonic generation due to picric acid impurity by Ghazaryan et al. [18]. In the best of our knowledge, no nanoindentation studies have been reported on GGP so far. Furthermore, as per the available literature, no theoretical investigations about their electro-optical and nonlinear optical (NLO) properties have been performed on GGP as well as GP molecules. The DFT, being a cost effective method, is very popular technique to determine reasonably well the vibrational frequencies (IR and Raman), molecular geometries, photophysical and NLO properties of different organic compounds as compared to the other conventional methodologies [5,6,24–34]. Therefore, the present work is based on experimental and theoretical investigations of various properties of GGP and GP (See structures in Fig. 1) and compared with experimental results wherever available. Therefore it is important to have a complete insight on various key properties of GP molecule, which we have studied computationally and discussed as analogue to GGP.

2. Experimental details

2.1. Synthesis and crystal growth

For synthesizing the glycine glycinium picrate (GGP) compound we have purchased picric acid and glycine materials from LOBA Chemicals Pvt. Ltd. The starting materials of

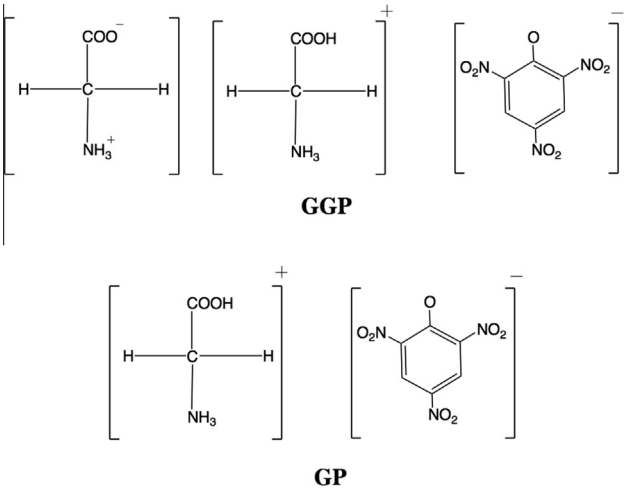

Figure 1 The structures of glycine glycinium picrate (GGP) (a) and glycinium picrate (GP) (b) molecules.

glycine and picric acid were taken in stoichiometric ratio (2:1) molar ratio. Initially the calculated amount of both the materials were taken in separate beaker and completely dissolved in double distilled water. After that a new beaker was taken and these materials were slowly mixed maintaining the temperature at nearly 40 °C for proper reaction. All the procedures were done in a Glove box and the colour of the mixed solution was observed as yellow. The chemical reaction mechanism involved in the synthesis of GGP is given as follows:

$$\underset{\text{Glycine}}{2(C_2H_5NO_2)} + \underset{\text{Picric acid}}{C_6H_3N_3O_7} \rightarrow \underset{\text{Glycine}}{(C_2H_5NO_2)} \times \underset{\text{glycinium}}{(C_2H_6NO_2)} . \underset{\text{picrate (GGP)}}{(C_6H_2N_3O_7)}$$

After proper chemical reaction the prepared solutions were allowed to evaporate at above the room temperature and get the yellow crystalline powder salt of GGP which was further used for crystal growth.

For single crystal growth of GGP, the slow evaporation method was employed: the very first step was to purify the synthesized materials for growth of high quality single crystals because the purity plays a vital role in crystal quality. Therefore, the synthesized material was purified by repeated recrystallization to get the material with high quality for crystal growth. Then the saturated solution of GGP was primed at 32 °C within three days by continuous stirring. The primed solution was then filtered in another beaker of high quality with a flat surface in closed air free environment. Later, it is sealed with a perforated lid and was aloof in a constant temperature bath at the same temperature for two days. After that

Please cite this article in press as: M. Shkir et al., A comparative study of key properties of glycine glycinium picrate (GGP) and glycinium picrate (GP): A combined experimental and quantum chemical approach, Journal of Saudi Chemical Society (2016), http://dx.doi.org/10.1016/j.jscs.2016.05.003

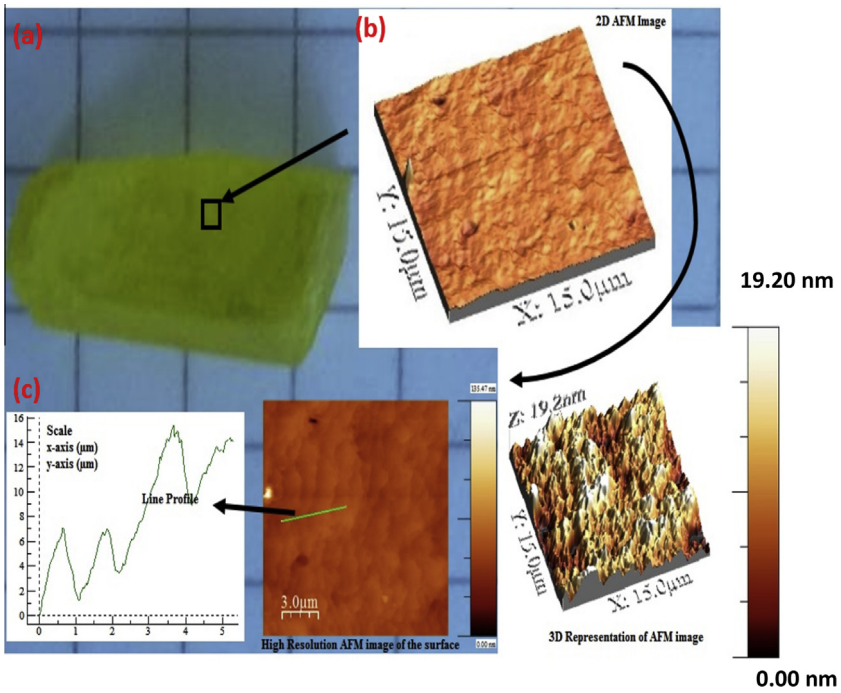

Figure 2 (a) As grown single crystal of GGP and (b) AFM image with 3D topography and (c) line profile for high resolution AFM image along (0 0 1) plane.

to the bath temperature was reduced gradually at the rate of 1 °C per day to reach room temperature (27 °C). During this period the growth process was monitored very carefully and a tiny nucleation was observed. Then within three weeks good quality single crystal of GGP [Fig. 2(a)] with reasonably good transparency was harvested from the mother solution and used for further characterizations along with AFM image with 3D topography [Fig. 2(b)] and line profile for high resolution AFM image along (0 0 1) plane [Fig. 2(c)].

2.2. Characterization techniques

The nanoindentation measurements were performed using a three-sided pyramidal Berkovich diamond indenter having nominal edge radius of 20 nm (faces 65.3° from vertical axis) attached to a fully calibrated nanoindenter (TTX-NHT, CSM Instruments). A high resolution AFM image for surface and line profile for roughness analysis for as grown GGP crystal was recorded before nanoindentation (insets to Fig. 1S). Later, the tests were carried out under load control to various peak loads in the range 5–150 mN with an approach speed of 2000 nm/min. The loading and unloading speed throughout the measurement was kept constant as 20 mN/min with 10 s of dwell time. A typical load-time sequence used for the present measurements is shown in the Fig. 1S. Totally 9 impressions (with varying load) were made at different places (distance between two impression is 50 μm) on an optically smooth surface of GGP single crystal along (0 0 1) direction. The inset to Fig. 1S shows the optical image of the imprint made using different loads. Standard Oliver and Pharr method was used for the analysis of the obtained results [35]. A commercial AFM (Ntegra Aura, NT-MDT) was used for taking topographic images of the surface.

3. Computational methodology

All the theoretical calculations on GGP and GP molecules were performed with Gaussian G09 package by adopting the default convergence principles, without any constraint on the geometry [36,37]. The ground state molecular geometries of GGP and GP molecules have been obtained from B3LYP/6-31G* level of theory. The B3LYP/6-31G* level of theory is usually considered a gateway choice to study the electro-optical properties of small molecule like GGP and GP [38–40]. The stable ground state optimized molecular geometries of GGP and GP are shown in Fig. 3 (Section 4.1). To obtain the equilibrium geometries of GGP and GP the self-consistent field equation was solved by achieving the true minimum on the potential energy surface (PES). To analyse all stationary points as global minima, their Infra-red (IR) and vibrational (Raman) frequencies have been calculated at the same B3LYP/6-31G* level of theory. Time-dependent density functional theory (TD-DFT) method has been used to calculate the absorption spectra. The solvent effects on absorption spectra have been simulated combining TD-DFT with polarizable continuum model (PCM). In the PCM model, the molecule is placed in a molecule-shaped cavity in the dielectric medium, the polarization effects on the solvated molecule being introduced through charges on the cavity surface. Finite Field (FF) method was applied to calculate the polarizability and static first hyperpolarizability (β_{tot}) along with their individual tensor components for titled compounds. The FF method was usually applied to study the NLO properties because it can be used in concert with the electronic structure method to work out β values. Recently, our calculated β amplitudes by FF method are found to be in reasonable agreement with other independent approaches for NLO calculations like two-level

Please cite this article in press as: M. Shkir et al., A comparative study of key properties of glycine glycinium picrate (GGP) and glycinium picrate (GP): A combined experimental and quantum chemical approach, Journal of Saudi Chemical Society (2016), http://dx.doi.org/10.1016/j.jscs.2016.05.003

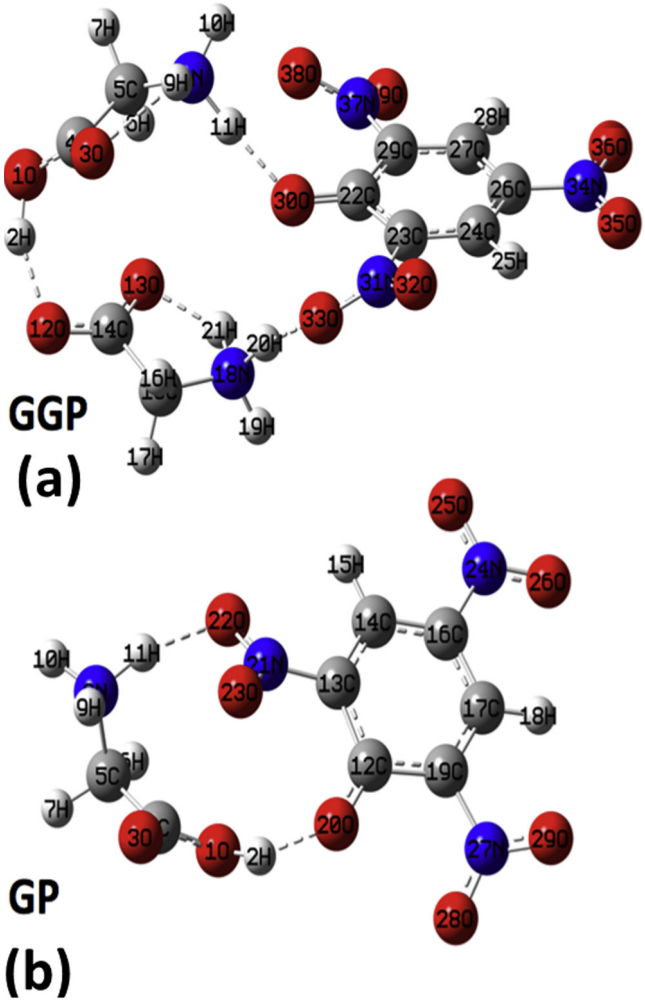

Figure 3 The ground state molecular geometries of (a) GGP and (b) GP molecules along with the numbering of atoms optimized at B3LYP/6-31G* level of theory.

model [41–43] as well as to the experimental EFISHG results. [44,45] In the FF method, a molecule is subjected to a static electric field (F) then the energy (E) is expressed by the following equation:

$$E = E^{(0)} - \mu_1 F_1 - \frac{1}{2}\alpha_{ij}F_iF_j - \frac{1}{6}\beta_{ijk}F_iF_jF_k - \frac{1}{24}\gamma_{ijkl}F_iF_jF_kF_l - \ldots \quad (1)$$

Here $E^{(0)}$ represents the total energy of molecule in the absence of an electric field, μ is the vector component of the dipole moment, α is the linear polarizability, β and γ are the second and third-order polarizabilities respectively, while x, y and z label the i, j, and k components, respectively. It can be seen from Eq. (1) that differentiating E with respect to F obtains the μ, α, β, and γ values.

4. Results and discussion

4.1. Molecular geometry analysis

The ground state optimized molecular geometries of GGP and GP molecules along with their numbering of atoms have been shown in Fig. 3. The important geometrical parameters including bond lengths and bond angles are collected in Tables 1S and 2S (see supplementary data). The optimized geometrical parameters of GGP molecule have also been compared with their experimental values as given in Table 1S (see supplementary data). The hydrogen bonding between glycine and picrate ionic species are represented by dotted lines as shown in Fig. 3. For the hydrogen bonding only those bond lengths are considered/shown in Fig. 3 that have less than 2 Å of bond distance between hydrogen bond donor and acceptor atoms. On the basis of intermolecular and intramolecular distances, five hydrogen bonds have been found for GGP. Among these five hydrogen bonds, three are intermolecular and two are intramolecular hydrogen bonds. The three intermolecular hydrogen bonds among picrate, glycinium ions include $O_{30}\ldots H_{11}$, $O_{33}\ldots H_{20}$ and $O_{12}\ldots H_2$ with their bond distances of 1.710 Å, 1.810 Å and 1.590 Å, respectively. On the basis of intra-atomic distances between hydrogen atom and hydrogen bond acceptor and the H-bond strength, it has several ranges e.g. strong (1.2–1.5 Å), medium (1.5–2.2 Å) or a weak (2.2–3.2 Å) hydrogen bond [46–48]. These values show that the hydrogen bonding is rationally medium between glycinium cation and picrate ion. The remaining two intramolecular hydrogen bonds of GGP molecule are between amino and acetate groups of glycine and glycinium dimer with its bond lengths of 1.686 Å and 1.983 Å, respectively. Unlike the GGP, in GP molecules there are only two intermolecular hydrogen bonds that have been observed between picrate anion and glycinium cation. These hydrogen bonds are $O_{22}\ldots H_{11}$ and $O_{20}\ldots H_2$ with their bond distances of 1.744 Å and 1.627 Å, respectively. A similar analysis of other bond lengths shows that most of the other bond lengths are also present in their usual standard ranges. For instance, the C—C, C—O, and C═O, bond lengths are within the range of standard values viz. 1.54 Å, 1.43 Å, 1.316 Å, respectively.

4.2. Vibrational analysis

Vibrational spectroscopy is a very strong tool in identifying the functional groups of organic, semi-organic, inorganic compounds as well as in molecular confirmation and reaction mechanism of new compounds. Fig. 2S (a1&a2) and (b1&b2) shows the infrared (IR) and Raman spectra of GGP and GP molecule calculated by DFT using B3LYP/6-31G* basis set, respectively. It is known that due to the combination of electron correlation effects and basis set deficiencies the theoretically calculated frequencies are found to be higher than the experimentally observed frequencies. Therefore, in the theoretically calculated frequencies we multiply by a suitable scaling factor of 0.9613 for B3LYP/6-31G* basis set [49,50]. The calculated frequencies were properly assigned and also compared with the same as well as other picrate compounds [18].

4.2.1. The comparative assessment of IR and Raman bands of GGP and GP

From Fig. 2S (a1&a2) [for GGP] and (b1&b2) [for GP] it is clear that the IR and Raman bands observed at ~3395, ~3187 cm^{-1} in both are due to NH asymmetric stretching of NH_3^+, at ~3101 and ~3005 in IR and 3135, 3066, 2997 in Raman are due to NH symmetric stretching vibrations of NH_3^+ in GGP, while these bands in GP are observed at ~3245, ~3137 cm^{-1}

and ~3083 cm^{-1} and ~3006 cm^{-1} respectively. The band observed in both IR and Raman spectra of GGP at ~2832, ~2737, 2590 cm^{-1} and GP at ~2799, ~2737, ~2806, ~2827, ~2837 cm^{-1} are due to sum tones. The IR and Raman bands observed in GGP and GP at ~1725, 1690 and ~1761 cm^{-1} can be assigned as stretching vibration of C═O in both COOH and asymmetric vibrations of COO group respectively.

Now all the peaks from the above explained peak down to 400 cm^{-1} for both GGP as well as GP are superimposed on a very broad band centered at ca. 1000 cm^{-1}, which is the characteristic of stretching vibrations of O–H bonds in case of strong hydrogen bonding O–H. . .O in GGP as well as GP, this hydrogen band is not present in Raman spectrum as usual as clear from Fig. 3(b). Both picric acid and picrates exhibit characteristic absorption peaks affected by C–C bond [51–55] similar to ones which are observed at 1639, 1621, 1587 cm^{-1} and 1640, 1622, 1604 cm^{-1} and 1668, 1630, and 1610, 1607 cm^{-1} in IR and Raman spectra of GGP and GP respectively. On the other hand both asymmetric stretching and deformation vibrations of COO^- and NH_3^+ groups are usually observed in this region so the above explained vibrational bands are may be caused by these vibrations too. The symmetric deformation vibrations of NH_3^+ group are usually observed near 1500 cm^{-1}. In both IR and Raman spectra of GGP and GP the nitro group has very active and characteristic vibrations. The presence of three such groups even more increases the intensity of the bands caused by this group. The vibrational assignment of nitro groups is done by most intensive peaks in Raman at 1543, 1509, 1440, 1415, 1336, 1320, 1258, 843 cm^{-1} in GGP and at 1553, 1515, 1453, 1415, 1345, 1330, 1299, 1253, 846 cm^{-1} in GP and their respective peaks in IR spectrum. The vibration modes at 1145, 1102, 1068, 920, 791 cm^{-1} in GGP while at 1145, 1099, 1076, 1061, 930, 899, 792, 776 cm^{-1} in GP observed in both IR and Raman respectively, are assigned to in plane deformation of CH, stretching of CN, ρ(CH_2), stretching of C–C, out of plane deformation of CH, wagging of NO_2, deformation of COO^-. The IR and Raman spectrum of GGP and GP contains the vibration peaks at 721 cm^{-1} and at 730 cm^{-1} and 722 cm^{-1} respectively is assigned to the wagging of NO_2 group. In IR and Raman spectra of GGP, the vibrations observed at 687 cm^{-1} while in GP at 700 cm^{-1} and 690 cm^{-1} are due to deformation of COO^- group. Vibrations observed in GGP at 540 cm^{-1} (IR) and 505 cm^{-1} (Raman) while in GP at 522 cm^{-1} (IR) and 520 cm^{-1} (Raman) are assigned to ρ(NO_2). The low intensity band observed at 471 cm^{-1} in both IR and Raman spectra of GGP while at 499 cm^{-1} in IR of GP respectively is assigned to ρ(COO^-) and below this band all are assigned as skeletal deformation and lattice vibration in the molecule. Thus as explained in above vibrational modes of GGP as well as GP, there is clear change in the peak positions and band appearances which concludes that GGP as well as GP both are different species and confirms their formation. The theoretically calculated all vibrational modes are comparable as well as found in close agreement with the experimental values of glycine glycinium picrate as well as glycinium picrate molecules [18].

4.3. Optical analysis

4.3.1. TD-DFT Study

To investigate the electronic transitions, oscillator strength and absorption spectra of GGP and GP molecules have been computed at TD-B3LYP/6-31G* level of theory. All the TD-DFT calculations have been performed on ground state optimized geometries in gas phase [56–59] as well as in different solvents. The investigation about solvatochromism behavior of GGP and GP has been carried out with different solvents effect through PCM model in water, acetone, cyclohexane and chloroform. The calculated values of absorption wavelength in the gas phase are found to be 396 nm and 483 nm for GGP and GP molecules, respectively. Interestingly, the solvatochromism is different for GGP and GP.

In the GGP molecule a slight effect of solvents on the absorption wavelengths has been observed, i.e., 11, 11, 7 and 10 nm, red shift in water, acetone, cyclohexane and chloroform compared to the gas phase, respectively, while in GP, there is a significant blue shift in absorption wavelength was noticed, i.e., 41, 39, 15 and 29 nm in water, acetone, cyclohexane and chloroform compared to the gas phase, respectively, see Table 1.

4.4. Nanoindentation examination

Fig. 4(a) shows the load–displacement curve (*P–h*) obtained for the present study. A smooth loading part was observed indicating a plastic deformation, which occurs underneath the indenter so as to accommodate the strain imposed by the sharp indenter. In addition a relatively homogeneous loading curve (for load below 100 mN) with no traces of any 'pop-in' features (i.e. discrete displacement bursts) except for a few serrations was observed. However, for load beyond 100 mN the pop-in events were observed with no pile-ups. The occurrence of this pop-in is related to the transition from elastic to elastic/-plastic regime, and is associated with the nucleation of plastic deformation due to dislocations and cracks [60]. A typical AFM image of the imprint made after indentation on (001) plane made by different load is shown in Fig. 4(b). Fig. 4(c) shows the cross section profile for the depth after indentation with different loads. A good correlation between the nanoindentation depth profile [Fig. 4(a)] and the profile from the AFM was seen [Fig. 4(c)]. Furthermore, an elastic deformation was evident from the curve during unloading half-cycle. During loading half cycle the recorded microhardness test showed a linear relation between P/h and h [Fig. 4(d)], which is consistent with the earlier studies [61]. The slope of the P/h–h curve is

Table 1 The calculated wavelength of maximum absorption (λ_a) in (nm), oscillator strength (f_o) and transition nature as calculated for GGP and GP with different solvation effects.

Solvents	GGP			GP		
	f_o	λ_a	Transition	f_o	λ_a	Transition
Gas	0.112	396	H → L (62%)	0.045	483	H → L (62%)
Water	0.139	407	H → L (69%)	0.098	442	H → L (67%)
Acetone	0.141	407	H → L (69%)	0.096	444	H → L (67%)
Cyclohexane	0.145	403	H → L (70%)	0.077	468	H → L (65%)
Chloroform	0.146	406	H → L (70%)	0.090	454	H → L (66%)

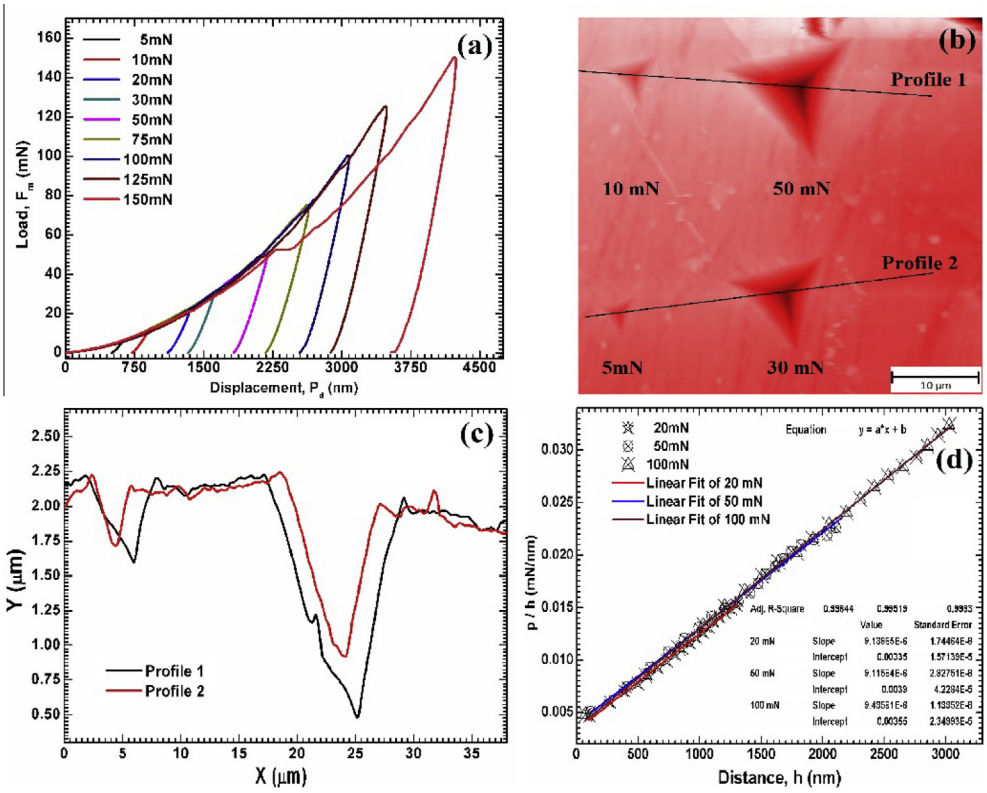

Figure 4 (a) Load displacement curve for the indentation measurement perpendicular to (0 0 1) (b) high resolution AFM image of indentation imprint (at different load) made on GGP surface along (0 0 1) plane, (c) its depth profile and (d) linear relation between P/h and h.

considered as a measure of load independent hardness, H_o i.e. $H_o = kb$, where k is a constant which depends on indenter geometry (1/24.5 for Berkovich indenter). The linear regression analysis of the curve was carried out and the value of 'b' for GGP single crystal was calculated which gave the value of load-independent hardness of about 458 MPa. The obtained p–h curve was then further analysed using various equations (described elsewhere [62] for obtaining various parameters associated with mechanical behavior of the GGP single crystal and is listed in Table 2.

4.4.1. Hardness analysis

The best fit calculated values of the hardness and Young's modulus of GGP crystals along (0 0 1) direction were plotted as a function of peak load [Fig. 5(a)]. A large scattering in the hardness value above 100 mN of load was observed, showing a load dependant parameter. This is due to inhomogeneous surface of the crystal and indentation size effect. Apart from this, a constant decrease in the hardness value of the sample with increasing load was observed. This suggests a significant indentation size effect on the value of hardness of the crystal. Further, this indentation size, d, which is proportional to the value of contact depth, h_c is related to the peak load as

$$P = a_0 + a_1 h_c + a_2 h_c^2, \tag{2}$$

where a_0, a_1 and a_2 are constants. Fig. 5(b) shows the variation of contact depth h_c with peak load. The curve is fitted with the as above polynomial function and the fitted value for a_0, a_1 and a_2 are shown in Fig. 5(b). The parameter a_2 is considered as a measure of the load-independent hardness H_0 and related to the empirical formula

Table 2 Various obtained parameters associated with the mechanical property of GGP single crystal along (0 0 1) plane.

Peak load, P_{max} (mN)	Hardness, H (MPa)	Young's modulus, E (MPa)	Vicker's Hardness	Displacement, h_{max} (nm)	Initially unloading stiffness, S (mN × nm^{-1})	Contact depth, h_c (nm)	m
5.04	688.6	18.308	63.772	608.39	0.0624	546	1.3
10.05	657.84	17.197	60.923	880.21	0.0848	788.76	1.3
20.04	560.13	15.696	51.874	1336.8	0.1186	1206.88	1.32
30.03	580.22	15.904	53.734	1611.42	0.1445	1451.69	1.33
50.05	521.24	14.621	48.273	2190.7	0.1812	1977.21	1.3
75.05	541.87	14.431	50.183	2642.75	0.2148	2374.71	1.34
100.07	527.56	14.664	48.858	3079.58	0.2554	2778.92	1.34
125.05	518.05	13.918	47.977	3486.92	0.2736	3134.89	1.31
150.07	404.48	13.275	37.459	4235.9	0.3237	3886.56	1.46

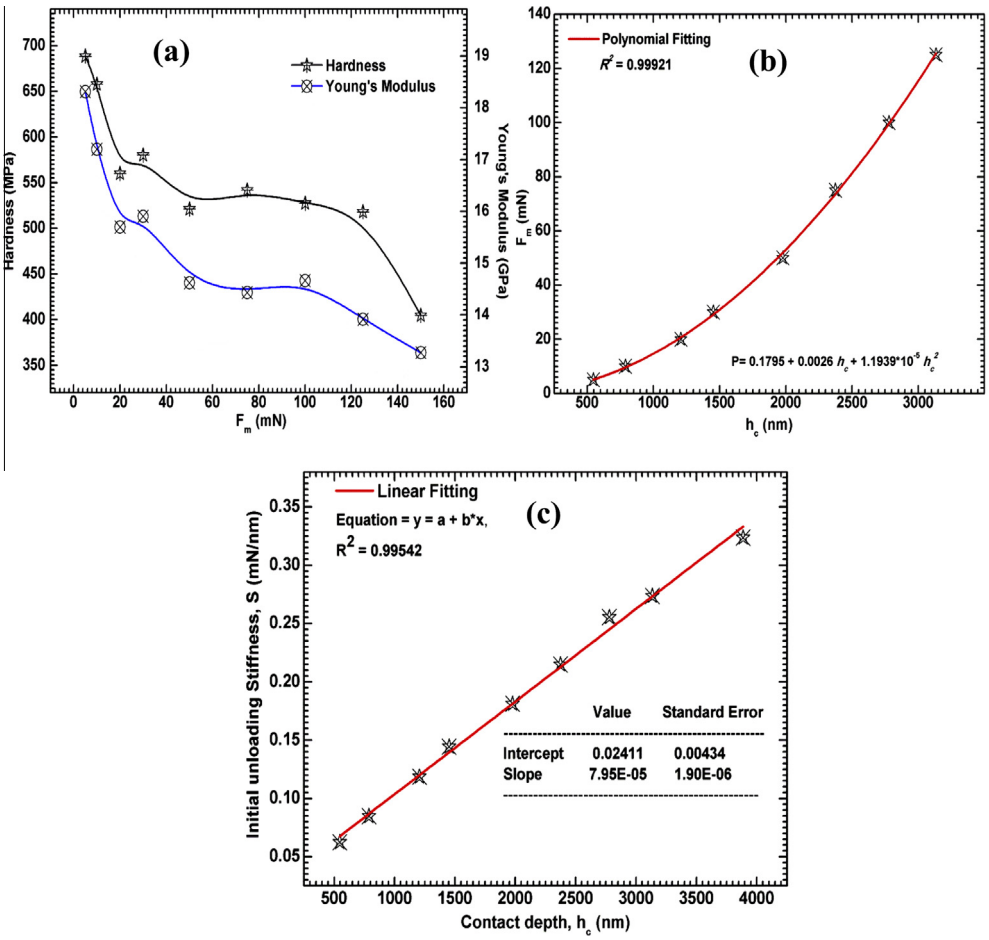

Figure 5 (a) Variation in the value of hardness and Young's modulus with varying load, (b) variation of contact depth (h_c) with peak load (F_n) and (c) Variation of initial loading stiffness (S) with contact depth (h_c).

$$H_0 = ka_2 \quad (3)$$

where, k is a constant which depends on the indenter geometry. For Berkovich indenter, used for the present study the value of k is 1/24.5. From the best fitted results obtained by fitting Fig. 5(b) using Eq. (4) gave a value a_2 as 1.1939×10^{-5} mN nm^{-2} Using this value the load-independent hardness for the present sample was calculated using Eq. (5) and found to be 480 MPa.

Fig. 5(c) below shows the variation of initial loading stiffness, S, with the contact depth at peak load, h_c. A linear relationship between the initial unloading stiffness, S and the contact dept at peak load was observed. The reduced Young's modulus was extracted from the slope of the linear fitted curve. The slope and the intercept in S-axis were found to be 0.0000795 mN nm^{-2} and 0.02411 mN nm^{-1}. The value of reduced Young's modulus as obtained from the slope of the curve was found to be ~80 GPa. Practically, the best fit curve should pass through the origin, however, a value higher than zero for intercept is related to the indenter tip rounding.

4.5. Differential scanning calorimetric (DSC) analysis

It is very important to know the thermal stability of any compound before using it for any device applications. For any optical system such as lasers, the thermal expansion, specific heat and thermal conductivity are the key parameters, therefore many scientists are continuously trying to find a material to grow their single crystals with high thermal stability. Hence, the differential scanning calorimetric (DSC) technique was used to know the thermal parameters of the grown crystals as it plays a key role to analyse the stability of materials and measures the temperature and heat flow associated with transitions in materials. The grown crystals were subjected to DSC measurements using a NETZSCH STA 449F3 Instruments in the temperature range 25–350 °C, at a heating rate of 10 °C min^{-1} and under air flow of 30 mL min^{-1}.

The DSC curve [Fig. 3S] is particularly characterized by one endothermic peak at ~212.6 °C which represents its melting point and the sharpness of the peak confirms that the crystals are of good crystallinity. Certain chemical changes such as oxidative degradations in any molecule are aided by exothermic peaks [63]. For further confirmation of its melting point, a melting point apparatus was used and the melting point was found to be ~211.7 °C. The high thermal stability and good crystallinity of the grown crystal signify that it can be useful for various optical applications.

4.6. Polarizability and first hyperpolarizability

We have used the DFT method to determine the electronic dipole moment (μ), polarizability (α_0), anisotropy

polarizability ($\Delta\alpha$) and first hyperpolarizability (β_{tot}) etc. of the GGP and GP molecules.

The electronic dipole moment can be calculated as:

$$\mu = (\mu_x^2 + \mu_y^2 + \mu_z^2)^{\frac{1}{2}} \quad (4)$$

Similarly, the average polarizability and anisotropic polarizability are defined as:

$$\alpha_0 = \frac{1}{3}(\alpha_{xx} + \alpha_{yy} + \alpha_{zz}) \quad (5)$$

$$\Delta\alpha = \frac{1}{\sqrt{2}}\sqrt{[(\alpha_{xx} - \alpha_{yy})^2 + (\alpha_{yy} - \alpha_{zz})^2 + (\alpha_{zz} - \alpha_{xx})^2 + 6\alpha_{xz}^2]} \quad (6)$$

Table 3 Calculated values of dipole moments (μ, Debye), polarizability (α, $\Delta\alpha$), and first hyperpolarizability (β_{tot}, β_0) with their individual tensor components for GGP and GP.

Components	GGP a. u.	GP a. u.	Components	GGP a. u.	GP a. u.
α_{xx}	235	226	β_{xxx}	777	−492
α_{xy}	−20	16	β_{xxy}	601	−860
α_{yy}	211	159	β_{xyy}	−435	79
α_{xz}	−39	27	β_{yyy}	−60	137
α_{yz}	27	−34	β_{xxz}	−246	407
α_{zz}	134	102	β_{xyz}	−283	−283
α_0	193	162	β_{yyz}	116	−31
$\Delta\alpha$	161	117	β_{xzz}	−5	230
μ_x	−2.891D	−5.571D	β_{yzz}	158	−78
μ_y	2.969D	−2.711D	β_{zzz}	−12	139
μ_z	0.383D	1.363D	β_0	427	582
μ_{tot}	4.162D	6.344D	β_{tot}	712	970

For first hyperpolarizability, its amplitude (β_{tot}) can be calculated using the x, y, z components as:

$$\beta_{tot} = \sqrt{(\beta_x^2 + \beta_y^2 + \beta_z^2)} \quad (7)$$

where these components are defined as:

$$\beta_x = (\beta_{xxx} + \beta_{xxy} + \beta_{xyy})$$
$$\beta_y = (\beta_{yyy} + \beta_{xxz} + \beta_{yyz})$$
$$\beta_z = (\beta_{xzz} + \beta_{yzz} + \beta_{zzz})$$

while β_0 can be also calculated by following relationship:

$$\beta_0 = \frac{3}{5}\beta_{tot} \quad (8)$$

It is well known that the first hyperpolarizability is a third rank tensor which can be described by a $3 \times 3 \times 3$ matrix. In the 3D matrix there are 27 components they are reduced to 10 components due to Kleinman symmetry [56], which can be given in lower tetrahedral format and is obvious that the lower part of $3 \times 3 \times 3$ matrices is tetrahedral. The amplitudes of polarizability and hyperpolarizability of any molecular system is dependent on the electronic communication of two different parts of molecular systems. We have collected all the calculated values of dipole moment, polarizability and first hyperpolarizability in Table 3.

The total value of dipole moment of GGP is found to be 6.344 D, which is ~2.182 D larger than that of the total dipole moment of GP. The calculated values of average polarizability α_0 are 193 and 162 a. u. while anisotropic polarizability $\Delta\alpha$ is 161 and 117 a. u. for GGP and GP, respectively. The amplitudes of calculated total first hyperpolarizability (β_{tot}) are 712 and 970 a. u. for GGP and GP, respectively. On comparing the first hyperpolarizability value of GGP and GP molecule with a prototype molecule of urea (β_{urea} = 43 a. u.), it is found that β_{tot} of GGP and GP are ~16 and 23 times larger than that of urea as calculated at the same levels of theory.

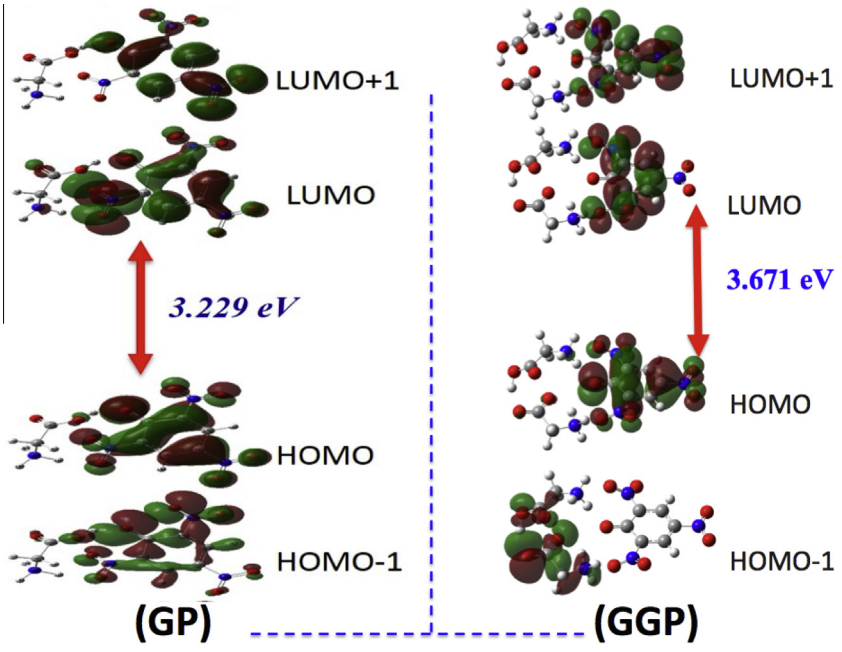

Figure 6 The frontier molecular orbitals of GP and GGP with an iso-value of ±0.02 a. u.

From the above results it is clear that GGP and GP can be used in various optoelectronic device applications with the advantage of their good transparency.

4.7. Frontier molecular orbitals (FMOs) analysis

The FMOs play a crucial role on the reactivity of any chemical system. For instance, the highest occupied molecular orbital (HOMO) and lowest unoccupied molecular orbital (LUMO) show the ability of donating and accepting the electron in any molecule, respectively. Several chemical properties of a molecule including chemical hardness, chemical potential, reactivity, kinetic stability, optical polarizability, chemical softness, electronegativity, electrophilicity etc. can be explained by FMOs. The FMOs have been drawn in Fig. 6 to get an intuitive view about their distribution patterns in GGP and GP molecules. In GGP, the HOMO and LUMO are localized at picrate anion and there is slight charge re-distribution with a relatively larger energy and having transition from HOMO to LUMO. On the other hand, in GP, the HOMO and LUMO have a relatively larger spread over the picrate anion as well as involving a slight part of glycinium. The transition with lower energy involves relatively larger re-distribution of charge from HOMO to LUMO orbitals, which perhaps results in relatively larger β_0 amplitude for GP as given in Table 3S (see supplementary data). Similarly, HOMO–LUMO (H–L) energy gaps have been also compared with each other as given in Table 3S (see supplementary data) and Fig. 6. The H–L energy gaps for GP and GGP are 3.229 and 3.761 eV, respectively. The lower H–L energy gap of GP causes its lower energy transitions, which perhaps results in larger β_0 amplitude for GP. Additionally, energy gaps of other orbitals have been given in Table 3S (see supplementary data).

To understand the relationship between structure, stability, and global chemical reactivity the global reactivity descriptors are used which can be calculated by density functional theory (DFT) study (details can be found in supporting information).

5. Conclusions

A comparative study of electro-optical properties for glycine glycinium picrate (GGP) and glycinium picrate (GP) compounds has been performed using a dual approach comprising of experimental and computational techniques. The single crystal of GGP has been grown using the slow evaporation technique and subjected to further experimental characterizations. The nanoindentation was used to study the load dependence and independence of hardness (H) and Young's modulus (E) using the Oliver–Pharr method and it was found that both H and E exhibit peak load dependence. The thermal stability of the GGP was assessed using DSC, which showed that it is stable up to 212 °C. Using the density functional theory (DFT) methods, we have also investigated its analogous GP molecule. The stable molecular geometry of GGP and GP was calculated at B3LYP/6-31G* level of theory. The experimental geometrical parameters of GGP have been reproduced by DFT at B3LYP/6-31G* level of theory. The slight inter-molecular charge transport has been observed from picrate anion to the glycinium cation, which leads to refrain the electro-optical properties, i.e., enhanced dipole moment, hyperpolarizability and tune the absorption wavelengths. It is expected that the inter-molecular charge transport might lead to the significant solvatochromic effect in GP. Similarly, the calculated amplitudes of first hyperpolarizability (β_{tot}) for GGP and GP are found to be 712 and 970 a. u., respectively, which are about 16 and 23 times larger than that of the urea molecule (a prototype NLO molecule). Thus, the present study highlights the optical and nonlinear optical properties of GGP and GP molecules. The non-zero and larger values of first hyperpolarizability is the most important parameter that might make GGP and GP molecules an outstanding aspirant for modern optoelectronic device applications.

Acknowledgments

The authors are highly thankful to King Khalid University for providing the necessary research facilities. Budhendra Singh would like to express their personal thanks to FCT (Fundação para a Ciência e a Tecnologia, Portugal, Funded by NSRF-POPH) for post-doctoral research Grants with reference numbers SFRH/BPD/76184/2011.

Appendix A. Supplementary data

Supplementary data associated with this article can be found, in the online version, at http://dx.doi.org/10.1016/j.jscs.2016.05.003.

References

[1] J.-P. Farges, Organic Conductors: Fundamentals and Applications, Marcel Dekker, 1994.
[2] T. Ishiguro, K. Yamaji, Organic Superconductors, 1990.
[3] B. Saleh, MC Teich Fundamentals of Photonics, John Wiley & Sons, New York, 1991.
[4] B.G. Penn, B.H. Cardelino, C.E. Moore, A.W. Shields, D. Frazier, Growth of bulk single crystals of organic materials for nonlinear optical devices: an overview, Prog. Cryst. Growth Charact. Mater. 22 (1991) 19–51.
[5] M. Shkir, H. Abbas, Physico chemical properties of l-asparagine l-tartaric acid single crystals: a new nonlinear optical material, Spectrochim. Acta Part A Mol. Biomol. Spectrosc. 118 (2014) 172–176.
[6] M. Shkir, H. Abbas, On the ground and excited state of glycine–glutaric acid: a new organic material, Spectrochim. Acta Part A Mol. Biomol. Spectrosc. 125 (2014) 453–457.
[7] D.R. Kanis, M.A. Ratner, T.J. Marks, Design and construction of molecular assemblies with large second-order optical nonlinearities, quantum chemical aspects, Chem. Rev. 94 (1994) 195–242.
[8] P.N. Prasad, D.J. Williams, Introduction to Nonlinear Optical Effects in Molecules and Polymers, Wiley, New York etc., 1991.
[9] M. Shkir, B. Riscob, M. Hasmuddin, P. Singh, V. Ganesh, M. Wahab, E. Dieguez, G. Bhagavannarayana, Optical spectroscopy, crystalline perfection, etching and mechanical studies on P-nitroaniline (PNA) single crystals, Opt. Mater. 36 (2014) 675–681.
[10] M. Shakir, S. Kushawaha, K. Maurya, S. Kumar, M. Wahab, G. Bhagavannarayana, Enhancement of second harmonic generation, optical and dielectric properties in L-asparagine monohydrate single crystals due to an improvement in crystalline perfection by annealing, J. Appl. Crystallogr. 43 (2010) 491–497.

[11] H. Tanak, Density functional computational studies on 2-[(2, 4-dimethylphenyl) iminomethyl]-3, 5-dimethoxyphenol, Int. J. Quantum Chem. 112 (2012) 2392–2402.
[12] M. Shkir, S. Muhammad, S. AlFaify, A. Irfan, I. Yahia, A dual approach to study the electro-optical properties of a noncentrosymmetric l-asparagine monohydrate, Spectrochim. Acta Part A Mol. Biomol. Spectrosc. 137 (2015) 432–441.
[13] M. Shkir, S. AlFaify, H. Abbas, G. Bhagavannarayana, A physico-chemical approach to study the experimental and theoretical properties of l-ornithine monohydrochloride: an organic nonlinear optical material, Mater. Chem. Phys. 155 (2015) 36–46.
[14] S.R. Marder, B. Kippelen, A.K.-Y. Jen, N. Peyghambarian, Design and synthesis of chromophores and polymers for electro-optic and photorefractive applications, Nature 388 (1997) 845–851.
[15] H. Ikeda, T. Sakai, K. Kawasaki, Nonlinear optical properties of cyanine dyes, Chem. Phys. Lett. 179 (1991) 551–554.
[16] H. Katz, K. Singer, J. Sohn, C. Dirk, L. King, H. Gordon, Greatly enhanced second-order nonlinear optical susceptibilities in donor-acceptor organic molecules, J. Am. Chem. Soc. 109 (1987) 6561–6563.
[17] D. Sajan, H. Joe, V. Jayakumar, J. Zaleski, Structural and electronic contributions to hyperpolarizability in methyl p-hydroxy benzoate, J. Mol. Struct. 785 (2006) 43–53.
[18] V. Ghazaryan, M. Fleck, A. Petrosyan, Glycine glycinium picrate—reinvestigation of the structure and vibrational spectra, Spectrochim. Acta Part A Mol. Biomol. Spectrosc. 78 (2011) 128–132.
[19] S. Thilagavathy, K. Ambujam, Growth of glycine picrate crystal by conventional and SR method, Trans. Indian Inst. Met. 64 (2011) 143–147.
[20] M. Shakir, S. Kushwaha, K. Maurya, M. Arora, G. Bhagavannarayana, Growth and characterization of glycine picrate—remarkable second-harmonic generation in centrosymmetric crystal, J. Cryst. Growth 311 (2009) 3871–3875.
[21] M. Shakir, B. Singh, B. Kumar, G. Bhagavannarayana, Ferroelectricity in glycine picrate: an astonishing observation in a centrosymmetric crystal, Appl. Phys. Lett. 95 (2009), 252902-252902-252903.
[22] T. Kai, M. GoTo, K. Furuhata, H. Takayanagi, Crystal structure of glycine picrate, Anal. Sci. 10 (1994) 359–360.
[23] T.U. Devi, N. Lawrence, R.R. Babu, K. Ramamurthi, Growth and characterization of glycine picrate single crystal, Spectrochim. Acta Part A Mol. Biomol. Spectrosc. 71 (2008) 340–343.
[24] B.G. Johnson, P.M. Gill, J.A. Pople, The performance of a family of density functional methods, J. Chem. Phys. 98 (1993) 5612–5626.
[25] M. Cinar, A. Coruh, M. Karabacak, A comparative study of selected disperse azo dye derivatives based on spectroscopic (FT-IR, NMR and UV–Vis) and nonlinear optical behaviors, Spectrochim. Acta Part A Mol. Biomol. Spectrosc. 122 (2014) 682–689.
[26] H. Abbas, M. Shkir, S. AlFaify, Density functional study of spectroscopy, electronic structure, linear and nonlinear optical properties of l-proline lithium chloride and l-proline lithium bromide monohydrate: For laser applications, Arabian J. Chem. (2015), http://dx.doi.org/10.1016/j.arabjc.2015.02.011.
[27] M. Shkir, H. Abbas, S. Kumar, G. Bhagavannarayana, S. AlFaify, Experimental and theoretical studies on bis (glycine) lithium nitrate (BGLiN): a physico-chemical approach, J. Phys. Chem. Solids 75 (2014) 959–965.
[28] M. Shkir, S. AlFaify, H. Abbas, S. Muhammad, First principal studies of spectroscopic (IR and Raman, UV-visible), molecular structure, linear and nonlinear optical properties of L-arginine p-nitrobenzoate monohydrate (LANB): a new non-centrosymmetric material, Spectrochim. Acta Part A: Mol. Biomol. Spectrosc. 147 (2015) 84–92.
[29] M. Shkir, S. Muhammad, S. AlFaify, Experimental and density functional theory (DFT): a dual approach to study the various important properties of monohydrated L-proline cadmium chloride for nonlinear optical applications, Spectrochim. Acta Part A: Mol. Biomol. Spectrosc. 143 (2015) 128–135.
[30] M. Arivazhagan, R. Meenakshi, Vibrational spectroscopic studies and DFT calculations of 4-bromo-o-xylene, Spectrochim. Acta Part A Mol. Biomol. Spectrosc. 91 (2012) 419–430.
[31] A. Reshak, W. Khan, The density functional study of electronic structure, electronic charge density, linear and nonlinear optical properties of single crystal alpha-LiAlTe 2, J. Alloy. Compd. 592 (2014) 92–99.
[32] K. Govindarasu, E. Kavitha, Vibrational spectra, molecular structure, NBO, UV, NMR, first order hyperpolarizability, analysis of 4-methoxy-4′-nitrobiphenyl by density functional theory, Spectrochim. Acta Part A Mol. Biomol. Spectrosc. 122 (2014) 130–141.
[33] S. Elleuch, H. Feki, Y. Abid, HF, MP2 and DFT calculations and spectroscopic study of the vibrational and conformational properties of N-diethylendiamine, Spectrochim. Acta Part A Mol. Biomol. Spectrosc. 68 (2007) 942–947.
[34] M. Shkir, S. Muhammad, S. AlFaify, A. Irfan, P.S. Patil, M. Arora, H. Algarni, Z. Jingping, An investigation on the key features of a D-[small pi]-A type novel chalcone derivative for opto-electronic applications, RSC Adv. 5 (2015) 87320–87332.
[35] W.C. Oliver, G.M. Pharr, An improved technique for determining hardness and elastic modulus using load and displacement sensing indentation experiments, J. Mater. Res. 7 (1992) 1564–1583.
[36] M.J. Frisch, G.W. Trucks, H.B. Schlegel, G.E. Scuseria, M.A. Robb, J.R. Cheeseman, G. Scalmani, V. Barone, B. Mennucci, G.A. Petersson, H. Nakatsuji, M. Caricato, X. Li, H.P. Hratchian, A.F. Izmaylov, J. Bloino, G. Zheng, J.L. Sonnenberg, M. Hada, M. Ehara, K. Toyota, R. Fukuda, J. Hasegawa, M. Ishida, T. Nakajima, Y. Honda, O. Kitao, H. Nakai, T. Vreven, J.A. Montgomery, J.E. Peralta, F. Ogliaro, M. Bearpark, J.J. Heyd, E. Brothers, K.N. Kudin, V.N. Staroverov, R. Kobayashi, J. Normand, K. Raghavachari, A. Rendell, J.C. Burant, S.S. Iyengar, J. Tomasi, M. Cossi, N. Rega, J.M. Millam, M. Klene, J.E. Knox, J.B. Cross, V. Bakken, C. Adamo, J. Jaramillo, R. Gomperts, R.E. Stratmann, O. Yazyev, A.J. Austin, R. Cammi, C. Pomelli, J.W. Ochterski, R.L. Martin, K. Morokuma, V.G. Zakrzewski, G.A. Voth, P. Salvador, J.J. Dannenberg, S. Dapprich, A.D. Daniels, Farkas, J.B. Foresman, J.V. Ortiz, J. Cioslowski, D.J. Fox, Gaussian 09, Revision B.01, Wallingford CT, 2009.
[37] H.B. Schlegel, Optimization of equilibrium geometries and transition structures, J. Comput. Chem. 3 (1982) 214–218.
[38] A.D. Becke, Density-functional thermochemistry. III. The role of exact exchange, J. Chem. Phys. 98 (1993) 5648–5652.
[39] C. Lee, W. Yang, R.G. Parr, Development of the Colle–Salvetti correlation-energy formula into a functional of the electron density, Phys. Rev. B 37 (1988) 785–789.
[40] W.N. Setzer, Conformational analysis of thioether musks using density functional theory, Int. J. Mol. Sci. 10 (2009) 3488–3501.
[41] S. Muhammad, T. Minami, H. Fukui, K. Yoneda, R. Kishi, Y. Shigeta, M. Nakano, Halide ion complexes of decaborane (B10H14) and their derivatives: noncovalent charge transfer effect on second-order nonlinear optical properties, J. Phys. Chem. A 116 (2012) 1417–1424.
[42] S. Muhammad, H. Xu, Y. Liao, Y. Kan, Z. Su, Quantum mechanical design and structure of the Li@B10H14 basket with a remarkably enhanced electro-optical response, J. Am. Chem. Soc. 131 (2009) 11833–11840.

Please cite this article in press as: M. Shkir et al., A comparative study of key properties of glycine glycinium picrate (GGP) and glycinium picrate (GP): A combined experimental and quantum chemical approach, Journal of Saudi Chemical Society (2016), http://dx.doi.org/10.1016/j.jscs.2016.05.003

[43] S. Muhammad, C. Liu, L. Zhao, S. Wu, Z. Su, A theoretical investigation of intermolecular interaction of a phthalimide based "on–off" sensor with different halide ions: tuning its efficiency and electro-optical properties, Theor. Chem. Acc. 122 (2009) 77–86.
[44] S. Muhammad, A. Irfan, M. Shkir, A.R. Chaudhry, A. Kalam, S. AlFaify, A.G. Al-Sehemi, A.E. Al-Salami, I.S. Yahia, H.L. Xu, How does hybrid bridging core modification enhance the nonlinear optical properties in donor-π-acceptor configuration? A case study of dinitrophenol derivatives, J. Comput. Chem. 36 (2015) 118–128.
[45] S. Muhammad, H. Xu, M.R.S.A. Janjua, Z. Su, M. Nadeem, Quantum chemical study of benzimidazole derivatives to tune the second-order nonlinear optical molecular switching by proton abstraction, PCCP 12 (2010) 4791–4799.
[46] G.A. Jeffrey, G.A. Jeffrey, An Introduction to Hydrogen Bonding, Oxford University Press, New York, 1997.
[47] S. Scheiner, Hydrogen Bonding: A Theoretical Perspective (Topics in Physical Chemistry), Oxford University Press, Oxford, 1997.
[48] C.L. Perrin, J.B. Nielson, Strong hydrogen bonds in chemistry and biology, Annu. Rev. Phys. Chem. 48 (1997) 511–544.
[49] M.W. Wong, Vibrational frequency prediction using density functional theory, Chem. Phys. Lett. 256 (1996) 391–399.
[50] J.B. Foresman, Æ. Frisch, Exploring chemistry with electronic structure methods: a guide to using Gaussian (1996).
[51] G. Keresztury, S. Holly, G. Besenyei, J. Varga, A. Wang, J. Durig, Vibrational spectra of monothiocarbamates-II. IR and Raman spectra, vibrational assignment, conformational analysis and ab initio calculations of S-methyl-N, N-dimethylthiocarbamate, Spectrochim. Acta Part A: Mol. Spectrosc. 49 (1993) 2007–2026.
[52] G. Keresztury, Raman spectroscopy: theory, Handbook of vibrational spectroscopy (2002).
[53] P. Srinivasan, M. Gunasekaran, T. Kanagasekaran, R. Gopalakrishnan, P. Ramasamy, 2,4,6-trinitrophenol (TNP): an organic material for nonlinear optical (NLO) applications, J. Cryst. Growth 289 (2006) 639–646.
[54] M.B. Mary, V. Sasirekha, V. Ramakrishnan, Spectral investigations of amino acid picrates, Spectrochim. Acta Part A Mol. Biomol. Spectrosc. 65 (2006) 414–420.
[55] M.B. Mary, V. Sasirekha, V. Ramakrishnan, Vibrational spectral analysis of dl-valine dl-valinium and dl-methionine dl-methioninium picrates, Spectrochim. Acta Part A Mol. Biomol. Spectrosc. 65 (2006) 955–963.
[56] D. Kleinman, Nonlinear dielectric polarization in optical media, Phys. Rev. 126 (1962) 1977.
[57] D. Jacquemin, J. Preat, E.A. Perpète, A TD-DFT study of the absorption spectra of fast dye salts, Chem. Phys. Lett. 410 (2005) 254–259.
[58] D. Jacquemin, J. Preat, M. Charlot, V. Wathelet, J.-M. André, E.A. Perpète, Theoretical investigation of substituted anthraquinone dyes, J. Chem. Phys. 121 (2004) 1736–1743.
[59] M. Cossi, V. Barone, Time-dependent density functional theory for molecules in liquid solutions, J. Chem. Phys. 115 (2001) 4708–4717.
[60] S.K. Jat, N. Vijayan, A. Krishna, J. Philip, S. Verma, I. Bdikin, B. Singh, G. Bhagavannarayana, S. Halder, Nucleation kinetics, growth, mechanical, thermal and optical characterization of sulphamic acid single crystal, CrystEngComm 15 (2013) 10034–10042.
[61] I. Bdikin, B. Singh, J.S. Kumar, M. Graca, A. Balbashov, J. Grácio, A. Kholkin, Nanoindentation induced piezoelectricity in $SrTiO_3$ single crystals, Scr. Mater. 74 (2014) 76–79.
[62] A. Krishna, N. Vijayan, S. Gupta, K. Thukral, V. Jayaramakrishnan, B. Singh, J. Philip, S. Das, K. Maurya, G. Bhagavannarayana, Key aspects of l-threoninium picrate single crystal: an excellent organic nonlinear optical material with a high laser-induced damage threshold, RSC Adv. 4 (2014) 56188–56199.
[63] R. Gopalan, P. Subramanian, K. Rengarajan, Elements of Analytical Chemistry, Sultan Chand & Sons, New Delhi, 2003.

Please cite this article in press as: M. Shkir et al., A comparative study of key properties of glycine glycinium picrate (GGP) and glycinium picrate (GP): A combined experimental and quantum chemical approach, Journal of Saudi Chemical Society (2016), http://dx.doi.org/10.1016/j.jscs.2016.05.003